Terahertz-driven hot Dirac fermion and plasmon dynamics in the bulk-insulating topological insulator math xmlns="http://www.w3.org/1998/Math/MathML">mrow>msub>mi>Bi/mi>mn>2/mn>/msub>msub>mi>Se/mi>mn>3/mn>/msub>/mrow>/math>

Bumjoo Lee, Chihun In, Jisoo Moon, Tae Hoon Kim, Seongshik Oh, Tae Won Noh, and Hyunyong Choi

Phys. Rev. B **105**, 045307 — Published 31 January 2022

DOI: 10.1103/PhysRevB.105.045307

Terahertz-Driven Hot Dirac Fermion and Plasmon Dynamics in Bulk-Insulating Topological Insulator Bi_2Se_3

Bumjoo Lee[1,2], Chihun In[2,3,4,5], Jisoo Moon[6], Tae Hoon Kim[2,3], Seongshik Oh[6,7], Tae Won Noh[1,2], and Hyunyong Choi[2,3*]

[1]Center for Correlated Electron Systems, Institute for Basic Science, Seoul 08826, Republic of Korea

[2]Department of Physics and Astronomy, Seoul National University, Seoul 08826, Republic of Korea

[3]Institute of Applied Physics, Seoul National University, Seoul 08826, Republic of Korea

[4]Department of Physics, Freie Universität Berlin, Berlin 14195, Germany

[5]Department of Physical Chemistry, Fritz-Haber-Institute of the Max-Planck-Society, Berlin 14195, Germany

[6]Department of Physics and Astronomy, Rutgers, The State University of New Jersey, Piscataway, New Jersey 08854, United States of America

[7]Center for Quantum Materials Synthesis, Rutgers, The State University of New Jersey, Piscataway, New Jersey 08854, United States

*Corresponding author: hy.choi@snu.ac.kr

For degenerately doped three-dimensional topological insulators (3D TIs), the interaction dynamics between Dirac fermions and collective charge oscillations (plasmons) are considerably complicated. In particular, the low-energy contribution near band inversion is largely obscure because of the bulk-surface interaction as well as the two-dimensional electron gas (2DEG). We have circumvented these issues by performing high-field terahertz (THz) pump-probe spectroscopy in bulk insulating Bi_2Se_3 TI micro-ribbon array structures. Plasmon blueshift of 11 % was found to occur within 4 ps under 0.433 MV/cm THz excitation compared to the near-equilibrium state. Although the conventional optical pump or engineered micro-ribbon TIs exhibits a similar plasmon blueshift, our observation is readily explained by the intrinsic plasmon behavior from the increased electronic temperature ($T_e \cong 1,430$ K) and reduced chemical potential ($\mu \cong 16$ meV) without considering extrinsic contributions. Our findings may apply to other classes of Dirac materials to investigate the coupled low-energy interactions with collective quasiparticles.

When materials with Dirac dispersion are driven out-of-equilibrium, they can host a variety of nonequilibrium quantum phenomena. In three-dimensional topological insulators (3D TIs), such dynamics near the band inversion, i.e., Dirac point, is of fundamental interests because the massless Dirac fermions on the topological surface state (TSS) and the massive bulk carriers coexist [1-3], in which the light-induced carriers exhibit nontrivial features, different from conventional band insulators or gapless graphene [4-12]. Indeed, this unique character of band topology has been predicted to host exotic phenomena, such as quantum-confined two-dimensional electronic gas (2DEG) [4,5,13], strong electromagnetic field-induced nonlinear optical responses [11,14], and surface photovoltage [7,8,10]. Furthermore, the TSS Dirac

fermions can couple to the collective oscillation of carriers, i.e., plasmons. The TI surface plasmons are of particular interest not only because of the density scaling law of Dirac quasiparticles [3], but also their resonance tunability, for instance, by quantum interference [9,15-17], optical [6], and terahertz excitation [11,18]. These phenomena are promising for novel topological photonics such as ultrafast modulators and metamaterial applications.

However, for TIs with a degenerate Fermi sea above bulk conduction band, the intertwined bulk-surface interaction is strongly enhanced [3,19,20]. On the other hand, for the bulk-insulating TIs [21], if the TSS Dirac fermions can be excited exclusively, they absorb the incident photon energy, leading to the increased electronic temperature (T_e) [11,22-25]. The interaction dynamics with Dirac plasmons are then supposed not to follow a temperature-independent density scaling law of bulk carriers [26] or bulk photodoping effect [6], but obey the nonlinear temperature dependence of two-dimensional (2D) Dirac fermions [23,24,27]. Prior studies including the near-equilibrium and nonequilibrium optical spectroscopies [6,9,11,28], however, were not able to distinguish these characteristics. Clearly, it is the high-field THz pump-probe spectroscopy that can resolve the Dirac fermion-plasmon interaction pathways, but such investigations have still been lacking to date.

In this Letter, we present time-resolved investigations of the nonequilibrium Dirac particles driven by intense THz excitation in bulk insulating Bi_2Se_3 TIs. The Bi_2Se_3 TIs used in this study were grown using molecular beam epitaxy, and the wafer-scale samples were fabricated into micro-ribbon arrays by photolithography and reactive ion etching. The samples consist of Bi_2Se_3 (30 QL) and $(Bi_{0.5}In_{0.5})_2Se_3$ (8 QL)/In_2Se_3(8 QL) buffer layer that have been grown on a 3” diameter, 500 μm thick Al_2O_3 (0001) substrate. Initial 3 QL Bi_2Se_3 seed layer was grown first at 135 °C, followed by the 8 QL In_2Se_3 at 260 °C. It was annealed to 550 °C, which evaporated out the seed layer. Then, the 8 QL $(Bi_{0.5}In_{0.5})_2Se_3$ and the active 30 QL Bi_2Se_3 were

deposited at 245 °C in sequence. After the sample was cooled to room temperature, 50 nm thick Se capping layer was deposited on top to protect the film against atmospheric aging effect [29,30]. The estimated Fermi level E_{F} was about 75 meV, according to the Hall measurement and the Fermi velocity v_{F} from previous angle-resolve photoemission spectroscopy measurements [29,31]. The Fermi level lies deep within the bulk gap (~300 meV), and the sample is truly bulk-insulating, as depicted in FIG. 1(a) and confirmed by THz conductivity (See *Supplementary S1* [32]). The wafer-scale sample is then cut into small pieces of 10 by 10 mm by a diamond cutter. The Se capping layer was removed by heating the sample to 200 °C for 10 min for the lithography process. The Bi_2Se_3 layer is patterned using photolithography and RIE etching. The photoresist was removed by acetone, and the buffer layer was consequently removed by heating at 200 °C for 10 min. The patterned TI arrays have micro-ribbon widths $L_0 = 4, 8, 20$ μm, and period $2L_0$, as depicted in FIG. 1(b). Micrometer-sized periodicity of the ribbon array provides the momentum required to excite the plasmon resonance in the terahertz range [6,9,11,28].

For the THz pump-probe spectroscopy, 800-nm, 35-fs pulses were delivered from a 1 kHz regenerative amplifier (Coherent® Astrella Amplifier, see *Supplementary S2* for the measurement system details [32]). The high-field THz pump with peak field amplitude 0.433 MV/cm and center frequency 0.64 THz was obtained by a tilted-pulse-front phase-matching method in a lithium niobate ($LiNbO_3$) crystal [33,34]. The peak field amplitude was measured by the electro-optic sampling [35] (See *Supplementary S2* [32]). The THz pump is focused on the TI sample with a full-width half-maximum of 1 mm. The TI micro-ribbon arrays are excited by this intense THz pump, as depicted in FIG. 1(b). After a finite pump-probe delay $\Delta\tau$, the pump-induced change $\Delta(1-\tilde{t}(\nu))$ was measured by a weak THz probe pulse. The THz pump polarization is parallel to the TI micro-ribbon to excite the Dirac fermions,

simultaneously minimizing the direct plasmon excitation [28]. The THz probe is generated and detected via optical rectification through a zinc telluride (ZnTe) crystal [36]. The THz probe is polarized perpendicular to the TI micro-ribbon arrays to measure the plasmon response [28]. We also performed the optical pump (1.55 eV) and THz probe spectroscopy on the same sample to compare the THz pump excitation. All spectroscopic measurements were conducted at a liquid nitrogen temperature of 78 K.

Figure 1(c) presents the near-equilibrium extinction ratio $E(\nu) = 1 - |\tilde{t}(\nu)|^2$ spectra of the TI micro-ribbon arrays without pump excitation. The spectra exhibit dressed plasmon responses arising from Fano-type interference of plasmon-phonon interaction, superimposed by a bare plasmon response without plasmon-phonon interaction [9,28,37]. The plasmon resonance frequency ν_{pl} shifts upward with the decreasing micro-ribbon array period $2L_0$. The lowest energy optical phonon ($\mathrm{E_{1u}}$ mode) shows a center frequency $\sim$ 2 THz. The solid lines in FIG. 1(c) are least-square fits using the plasmon-phonon interaction model suggested by Giannini *et al.* [37] (See *Supplementary S3* for the detailed fitting analysis [32,38-40]). The dashed lines in FIG. 1(c) are the dressed plasmon (orange) by plasmon-phonon interaction and bare plasmon (blue) responses, respectively. The Fano-type interference of plasmon-phonon interaction shows nontrivial changes in the interaction coefficients with the different bare plasmon frequencies.

Figure 2(a) shows the THz pump-induced $\Delta(1 - \tilde{t}(\nu))$ spectra measured at $\Delta\tau$ of 3.0 and 3.6 ps (See *Supplementary S4* for the raw THz time-trace [32]). We choose this delay to avoid the coherent artifacts occurring near zero-time delay as well as to observe the thermalized state [41,42]. The peak and dip structure near 2 THz in the real and imaginary $\Delta(1 - \tilde{t}(\nu))$ show asymmetric line-shape, which intuitively originate from the Fano-type asymmetric oscillator, not from a symmetric Lorentzian oscillator [43]. Compared to the near-equilibrium state, the

differential $\Delta(1-\tilde{t}(\nu))$ exhibits $\Delta\nu_{\mathrm{pl}}/\nu_{\mathrm{pl}}$ of 11 % on average. The dotted blue and orange lines show the bare plasmon response before and after the THz pump excitation. The intense THz radiation leads to a substantial increase of T_{e}, which is similarly observed in graphene [23-25] as well as TI [11,22]. The corresponding change of chemical potential $\mu(T_{\mathrm{e}})$ is plotted in FIG. 2(b). Then, we obtain $\nu_{\mathrm{pl}}(k, T_{\mathrm{e}})$ as a function of k for different T_{e}, where k is the Dirac plasmon wavevector (See *Supplementary S5* for the detailed calculation [27,32,44]). Figure 2(c) displays $\nu_{\mathrm{pl}}(k, T_{\mathrm{e}})$ when T_{e} is 78 K (solid red line) and 1,430 K (solid black line), on top of which the experimentally determined ν_{pl} shift is shown (filled circles). We see that $\nu_{\mathrm{pl}}(k, T_{\mathrm{e}} = 1{,}430\ \mathrm{K})$ follows a nonlinear dependence of k, and ν_{pl} shifts to the higher frequency with increasing T_{e}.

We note that the THz-field-induced hot Dirac fermions are not the only way of turning ν_{pl}. Figure 3(a) shows the E difference between the samples with varying the width of micro-ribbon arrays without pump excitation. In this near-equilibrium regime, ν_{pl} blueshift can be understood by the plasmon excitations of oscillating Dirac fermions, as revealed in prior studies [45-47]. Other similar experiments have further revealed that the electric [48], magnetic [46,49], and thermodynamic interaction [23] play key roles in controlling ν_{pl}. Although engineering the width of TI micron-ribbon arrays shows interesting topological nature of plasmon scatterings, i.e., small contributions of edge effects [9] or Landau damping [9,28], which are typically occurred in conventional metal [50,51] or graphene [27,52,53], such results are all within the framework of interacting cold Dirac fermions. The others are experiments performed in a nonequilibrium regime, where femtosecond high-energy pulses are injected across the inverted gap [18,23,24,54]. Figure 3(b) shows $\Delta(1-\tilde{t}(\nu))$ spectra in the THz range, pumped by a 1.55-eV, 50-fs optical pulse. Despite similar ν_{pl} blueshifts and spectral features are

observed, the physical origin is distinct from either near-equilibrium or THz-pump cases, where the photo-induced bulk carriers experience multipath dynamics with the underlying 2DEG or the coupling to α phonon [6,9].

The observations above preclude several extrinsic contributions other than the contribution of single-particle hot Dirac fermions to the ν_{pl} blueshift in our THz pump-probe experiment. First, because the bulk energy gap (about 200 meV) is sufficiently larger than the THz photon energy (about 4 meV) and the Fermi level (about 75 meV), the bulk-surface interaction is fundamentally prohibited. Second, there is no interband contribution within the TSS Dirac cone. This is because the THz pump has photon energy much smaller than E_{F} so that the interband transitions are not allowed and Pauli-forbidden. Third, 2DEG contributions are unlikely to occur because the surface Fermi level is far below the conduction band such that the surface accumulated 2DEG should be absent [29,55]. Indeed, we find there is no experimental evidence of bulk photodoping effects in our THz pump-probe experiment (See *Supplementary S6* [32]).

The effect of T_{e} enhancement can be further analyzed by examining T_{e}-dependent $\mu(T_{\mathrm{e}})$ of 2D Dirac fermions. When the THz pump is $0.433\ \mathrm{MV/cm}$, we estimate T_{e} of 1,430 K. Because of the linear energy dependence of TSS density of states, $\mu(T_{\mathrm{e}})$ decreases with increasing T_{e} to satisfy the charge conservation. Numerical simulation of FIG. 2(b) indeed shows that $\mu(T_{\mathrm{e}})$ decreases to 16 meV at 1,430 K from 75 meV at 78 K. As a result, in the high-temperature limit $T_{\mathrm{e}} \gg T_{\mathrm{F}}$, where T_{F} is the TSS Fermi temperature, the thermal population of Dirac fermions dominates the plasmon response, similar to the undoped 2D Dirac carriers in graphene. We estimate T_{F} of 870 K from $T_{\mathrm{F}} = E_{\mathrm{F}}/k_B$ where k_B is the Boltzmann constant. Under finite doping, Das Sarma *et al.* [27] demonstrated that the Dirac plasmon resonance in the high-temperature and long-wavelength limit, i.e., $kv_F \ll \nu$, where ν is photon energy, is expressed as,

$$\nu_{pl} \propto \sqrt{k_B T_e \left(1 + \frac{T_F^4}{128(\ln 2)^3 T_e^4}\right)}, \quad (1)$$

from which the ν_{pl} blueshift is expected with increasing T_e. The expectation is consistent with our explanation that the experimental ν_{pl} shift shown in FIG. 2(c) can be understood solely by the increased T_e. In this high-temperature limit, the plasmon behavior is qualitatively different from the low-temperature behavior dominated by the doped carriers [27]. When T_e is smaller than T_F, $\mu(T_e)$ decreases, resulting in ν_{pl} redshift [27]. This scenario in the low-temperature limit obeys the following Sommerfeld expansion,

$$\nu_{pl} \propto \sqrt{E_F \left(1 - \frac{\pi^2}{6}\frac{T_e^2}{T_F^2}\right)}. \quad (2)$$

We note that such ν_{pl} redshift can be observed for T_e up to a temperature near T_F, as recently reported by Di Pietro *et al.* [11] In fact, the above two regimes, i.e., whether T_e dependence of ν_{pl} is redshifted or blueshifted, have been applied for graphene systems to understand the unusual T_e dependence of the Drude weight [23,24,54,56,57]. Because the light-induced hot Dirac fermions can change $\Delta\nu_{pl}$ polarity in both directions, our experimental results of $\nu_{pl}(k, T_e)$ dynamics and other reported studies [6,11,23,24,54] are fully consistent, whether T_e is above or below the T_F boundary.

The above discussion is limited to the THz-induced TSS and Dirac plasmons. To complete the story, we compare the results to the optically-excited THz dynamics. In FIGs. 4(a) and (b), we see that the THz-pumped signals exhibit much slower rising transients compared to the optically-pumped case. The time-dependent ν_{pl} shifts were obtained by fitted curves shown in FIGs. 4(c) and (d), which show good agreements with experimental $\Delta(1 - \tilde{t}(\nu))$. We attribute the rising dynamics of the THz pump-induced ν_{pl} shift to the increased T_e, as discussed above. If the pump photon energy is well below the lowest optical phonon energy

(i.e., α phonon of $f_{\mathrm{ph}} \cong 2$ THz), the absorbed THz photon energy is dissipated into the electrons across the 2D Dirac cone, before being dissipated into other degrees of freedoms, e.g., lattice [58-61] or defect [60]. In a similar condition on graphene, the low-energy pump-induced dynamics exhibit longer relaxation in the 25 and 300 ps range [59]. The THz pump-induced ν_{pl} shift in FIG. 4(c) indeed similarly slows down the relaxation time, compared to the optical pump-induced ν_{pl} shift in FIG. 4(b). The electron heat capacity C_{p} becomes proportional to T_{e} [11,62] as

$$C_{\mathrm{p}} = \gamma T_{\mathrm{e}}, \tag{3}$$

where γ is the Sommerfeld coefficient. Then the electron temperature follows a simple equation [11,62]

$$T_{\mathrm{e}}(\tau) = \sqrt{\frac{2I(\tau)}{\gamma} + T_0^2}, \tag{4}$$

where $I(\tau)$ is the absorbed THz pump power at $T_0 = 78$ K. Taking into account the THz pulse widths of 1–2 ps (See *Supplementary S2* and *S5* [32]), we see the estimated ν_{pl} shifts in FIG. 4(a) show a good agreement with the experimental observations. For the optical pump and THz probe case, on the other hand, the origin of ν_{pl} shift is primarily due to the photodoping effect. The rising dynamics of the optical pump-induced THz changes shown in FIG. 4(b) are similar to the previous reports from Sim *et al.* [6] and In *et al.* [9] The decaying transients are rather faster than these prior reports. We did not observe the long-lived surface photovoltage [7,8,10,55] in our samples. As suggested by Brahlek *et al.* [55], the solution of a steady-state Poisson equation shows that the length scale of the band bending is comparable to or greater than our sample thickness. Because no long relaxation dynamics [7,8,10] are observed in our optically pumped THz transients, it corroborates that the spatial separation of the photoexcited electron-hole pair, i.e., the origin of surface photovoltage effect, is negligible.

In conclusion, we have performed the time-resolved studies of nonequilibrium TI Dirac fermion-plasmon interaction by employing intense THz-pump excitation. We observed the transient blueshift of Dirac plasmons, reaching 11 % changes after the THz pump. The Dirac plasmon blueshift can be understood as a direct consequence of the hot Dirac fermions when T_e is well above the T_F bound. The high T_e from the intense THz pump correspondingly accompanies the transient reduction of μ, analogous to the undoped graphene [27], whereby the Dirac plasmon blueshift follows the induced thermal population. The THz-pump results further distinguish from the optical pump-induced ones, in which the former can be explained without considering the complicated extrinsic effects, such as bulk-surface interaction or 2DEG. Our work provides a crossover toward a unique platform, intrinsic Dirac plasmon, in studying fundamental photoinduced phenomena and timescales on the Dirac plasmon of TIs.

Acknowledgments

B.L., and T.W.N. are supported by the Institute for Basic Science (IBS) in Korea (grant no. IBS-R009-D1). C.I., T.H.K, and H.C. are supported by the National Research Foundation of Korea (NRF) grant funded by the Korea government (MSIT, MEST) (grant no. 2018R1A2A1A05079060, 2019R1A6A1A10073437, 2020M3F3A2A03082472, 2021R1A2C3005905), Creative Materials Discovery Program (grant no. 2017M3D1A1040828), Scalable Quantum Computer Technology Platform Center (grant no. 2019R1A5A1027055), and IBS in Korea (grant no. IBS-R014-G1-2018-A1). H.C. was supported by the New Faculty Startup Fund from Seoul National University. J.M. and S.O. were supported by MURI W911NF2020166 and the National Science Foundation (NSF) (grant no. DMR2004125).

Author contributions

B.L. and C.I. contributed equally to this work. H. C. conceived and supervised the work. B.L. performed the high-field THz and optical pump-probe measurement with the support of T. H. K. C.I. and B.L. performed the numerical calculation. J.M. and S.O. prepared the Bi_2Se_3 thin film sample and performed the sample characterizations. T. W. N. discussed the main result. B.L. and H.C. wrote the manuscript with the help of all authors. All authors discussed the results and commented on the manuscript.

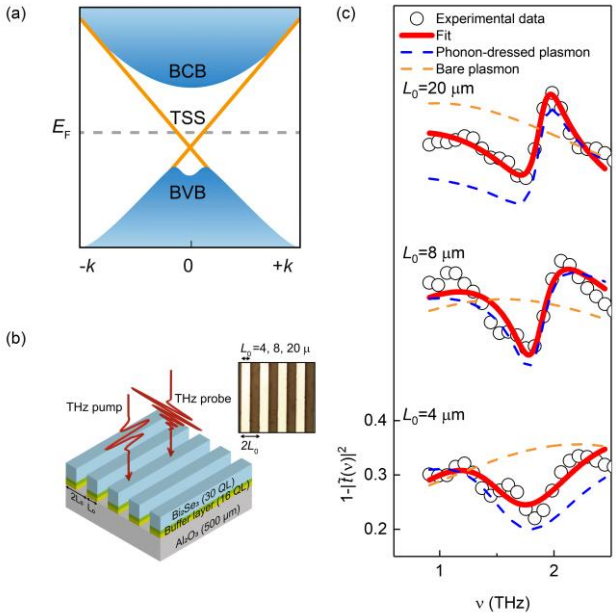

Figure 1 (a) A schematic band diagram of the bulk-insulating TIs (See *Supplementary S1* [32]). The topological surface state (TSS, solid orange lines), bulk conduction band (BCB), and bulk valence band (BVB) are shown. The Fermi energy (gray dotted line) of our sample is located at $E_F \cong 75$ meV above the Dirac point. The Fermi level of our sample lies deep within the bulk gap (200 meV). (b) A schematic of the THz pump-probe spectroscopy (See *Supplementary S2* [32]) on patterned TI micro-ribbon arrays with widths $L_0 = 4, 8, 20$ μm, and periods $2L_0$. The inset shows an optical microscopy image of our sample. The THz pump (probe) is polarized parallel (perpendicular) to the micro-ribbon array. (c) Near-equilibrium extinction coefficient ($E(\nu) = 1 - |\tilde{t}(\nu)|^2$, empty circles) of the TI micro-ribbon arrays and fitted curves (solid red lines, see *Supplementary S3* [32]). The samples with $L_0 = 20, 8, 4$ μm have plasmon resonance frequencies $\nu_{pl} = 0.98, 1.56, 2.20$ THz from the calculation (See *Supplementary S5* [32]). The bare plasmon and phonon-dressed plasmon from plasmon-phonon interaction are superimposed, where the Fano-type interaction creates an asymmetric oscillator near the IR-active α phonon (center frequency f_{ph} of ~ 2 THz, E_{1u}). The phonon-dressed plasmon responses (dotted blue lines) and the bare plasmon responses (dotted orange lines) are

displayed with offsets of 0.2 and 0.1, respectively.

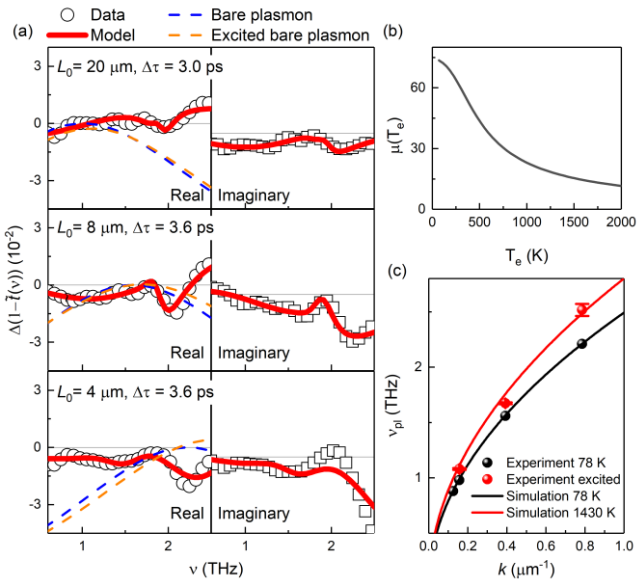

Figure 2 The THz pump-induced $\Delta(1-\tilde{t}(\nu))$ spectra and the corresponding numerical results. (a) The real and imaginary parts of $\Delta(1-\tilde{t}(\nu))$ spectra (empty circles) induced by the THz pump are shown together with the fitted curves (solid red line, see *Supplementary S3* for fitting details and *Supplementary S4* for the raw THz time-traces [32]). The plasmon resonance frequencies ν_{pl} show blueshifts of 11 % on average under THz pump excitation. The bare plasmon responses in near-equilibrium (dotted blue) and after THz pump-excitation (dotted orange) are overlapped. The dotted blue lines are displayed with normalization to have the amplitude of 10 % and offset -10 %. The dotted orange lines are scaled by the same ratio as blue dotted lines. (b) Calculated chemical potential $\mu(T_e)$ with increasing T_e. $\mu(T_e)$ decreases to 16 meV at 1,430 K, from 75 meV at 78 K. (c) The numerically calculated ν_{pl} with T_e of 78 K (solid black line) and 1,430 K (solid red line) are displayed. The experimental results from the near-equilibrium state (filled black circles) and excited state (filled red circles) are overlapped. (See *Supplementary S5* for calculation details [32])

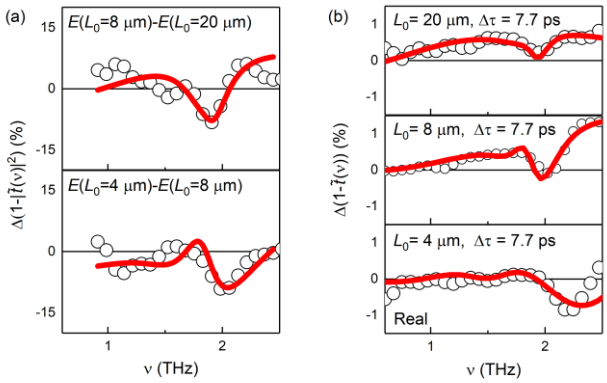

Figure 3 The experimental $\Delta E(\nu)$ and $\Delta(1-\tilde{t}(\nu))$ spectra by the structural engineering and the optical pump. (a) Differential near-equilibrium $\Delta E(\nu)$ spectra obtained by THz time-domain spectroscopy (empty circles). Each ΔE is obtained by subtracting E for $L_0 = 20$ μm from E for $L_0 = 8$ μm (upper panel), and E for $L_0 = 8$ μm from E for $L_0 = 4$ μm (lower panel). The evaluated spectra correspond to ν_{pl} blueshift of 50 % on average. The spectra are well explained by the differences (solid red lines) of the fitted curves shown in FIG. 1(c). (b) The optical pump-induced $\Delta(1-\tilde{t}(\nu))$ spectra (empty circles) with the fitted curves (solid red lines). ν_{pl} shows blueshifts of 8 % on average under 1.55-eV, 50-fs optical pump excitation (See *Supplementary S3* [32]).

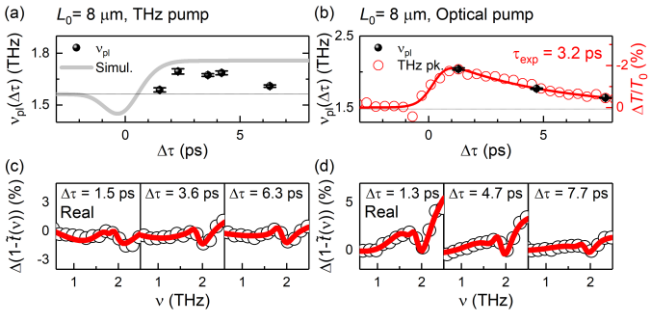

Figure 4 Time-resolved dynamics of ν_{pl} and $\Delta(1-\tilde{t}(\nu))$ spectra are compared for the THz- and optical-pump excitation. (a) The experimental measurements (filled black circles) and the model simulations (solid gray lines) of THz pump-induced ν_{pl} shifts. ν_{pl} shifts exhibit a slow rising behavior that appears up to ~ 4 ps. We simulate the rising time of ν_{pl} with pure T_e enhancement from THz pump absorption without relaxation (See Eq. 4 and *Supplementary S5* [32]). (b) The experimental measurements of optical pump-induced ν_{pl} shifts (filled black circles). The optical pump-induced THz peak transmission changes (empty red circles) show an exponential decay (solid red line) with a time constant of 3.2 ps. (c) Temporal evolution of the THz pump-induced $\Delta(1-\tilde{t}(\nu))$ spectra (empty circles) obtained for a sample of $L_0 = 8$ μm with fitted curves (solid red lines, see *Supplementary S3* [32]). (d) Temporal evolution of optical (1.55 eV) pump-induced $\Delta(1-\tilde{t}(\nu))$ spectra (empty circles) measured at the same sample as (c) with fitted curves (solid red lines, see *Supplementary S3* [32]). As a result of the slow rising and relaxation of THz pump-induced dynamics compared to the optical pump, the optical pump-induced change at $\Delta\tau = 7.7$ ps is comparable to the both THz pump-induced changes at $\Delta\tau = 3.6, 6.3$ ps

References

[1] M. Z. Hasan and C. L. Kane, Rev. Mod. Phys. **82**, 3045 (2010).

[2] C. L. Kane, *Topological Insulators: Chapter 1. Topological Band Theory and the □2 Invariant* (Elsevier Science, 2013).

[3] T. O. Wehling, A. M. Black-Schaffer, and A. V. Balatsky, Adv. Phys. **63**, 1 (2014).

[4] M. S. Bahramy, P. D. King, A. de la Torre, J. Chang, M. Shi, L. Patthey, G. Balakrishnan, P. Hofmann, R. Arita, N. Nagaosa et al., Nat. Commun. **3**, 1159 (2012).

[5] E. Wang, H. Ding, A. V. Fedorov, W. Yao, Z. Li, Y.-F. Lv, K. Zhao, L.-G. Zhang, Z. Xu, J. Schneeloch et al., Nat. Phys. **9**, 621 (2013).

[6] S. Sim, H. Jang, N. Koirala, M. Brahlek, J. Moon, J. H. Sung, J. Park, S. Cha, S. Oh, M. H. Jo et al., Nat. Commun. **6**, 8814 (2015).

[7] M. Neupane, S. Y. Xu, Y. Ishida, S. Jia, B. M. Fregoso, C. Liu, I. Belopolski, G. Bian, N. Alidoust, T. Durakiewicz et al., Phys. Rev. Lett. **115**, 116801 (2015).

[8] Y. Ishida, T. Otsu, T. Shimada, M. Okawa, Y. Kobayashi, F. Iga, T. Takabatake, and S. Shin, Sci. Rep. **5**, 8160 (2015).

[9] C. In, S. Sim, B. Kim, H. Bae, H. Jung, W. Jang, M. Son, J. Moon, M. Salehi, S. Y. Seo et al., Nano Lett. **18**, 734 (2018).

[10] T. Yoshikawa, K. Sumida, Y. Ishida, J. Chen, M. Nurmamat, K. Akiba, A. Miyake, M. Tokunaga, K. A. Kokh, O. E. Tereshchenko et al., Phys. Rev. B **100**, 165311 (2019).

[11] P. Di Pietro, N. Adhlakha, F. Piccirilli, A. Di Gaspare, J. Moon, S. Oh, S. Di Mitri, S. Spampinati, A. Perucchi, and S. Lupi, Phys. Rev. Lett. **124**, 226403 (2020).

[12] K. I. Bolotin, K. J. Sikes, Z. Jiang, M. Klima, G. Fudenberg, J. Hone, P. Kim, and H. L. Stormer, Solid State Commun. **146**, 351 (2008).

[13] B. C. Park, T. H. Kim, K. I. Sim, B. Kang, J. W. Kim, B. Cho, K. H. Jeong, M. H. Cho,

and J. H. Kim, Nat. Commun. **6**, 6552 (2015).

[14] K. J. A. Ooi and D. T. H. Tan, Proc. R. Soc. A. **473**, 20170433 (2017).

[15] M. Autore, F. D'Apuzzo, A. Di Gaspare, V. Giliberti, O. Limaj, P. Roy, M. Brahlek, N. Koirala, S. Oh, F. J. García de Abajo et al., Adv. Opt. Mater. **3**, 1257 (2015).

[16] Y. D. Glinka, S. Babakiray, T. A. Johnson, and D. Lederman, J. Phys. Condens. Matter **27**, 052203 (2015).

[17] S. Sim, N. Koirala, M. Brahlek, J. H. Sung, J. Park, S. Cha, M.-H. Jo, S. Oh, and H. Choi, Phys. Rev. B **91**, 235438 (2015).

[18] L. Luo, X. Yang, X. Liu, Z. Liu, C. Vaswani, D. Cheng, M. Mootz, X. Zhao, Y. Yao, C. Z. Wang et al., Nat. Commun. **10**, 607 (2019).

[19] N. P. Butch, K. Kirshenbaum, P. Syers, A. B. Sushkov, G. S. Jenkins, H. D. Drew, and J. Paglione, Phys. Rev. B **81**, 241301(R) (2010).

[20] D. Culcer, Physica E: Low. Dimens. Syst. Nanostruct. **44**, 860 (2012).

[21] R. Valdes Aguilar, A. V. Stier, W. Liu, L. S. Bilbro, D. K. George, N. Bansal, L. Wu, J. Cerne, A. G. Markelz, S. Oh et al., Phys. Rev. Lett. **108**, 087403 (2012).

[22] Y. H. Wang, D. Hsieh, E. J. Sie, H. Steinberg, D. R. Gardner, Y. S. Lee, P. Jarillo-Herrero, and N. Gedik, Phys. Rev. Lett. **109**, 127401 (2012).

[23] M. Wagner, Z. Fei, A. S. McLeod, A. S. Rodin, W. Bao, E. G. Iwinski, Z. Zhao, M. Goldflam, M. Liu, G. Dominguez et al., Nano Lett. **14**, 894 (2014).

[24] A. J. Frenzel, C. H. Lui, Y. C. Shin, J. Kong, and N. Gedik, Phys. Rev. Lett. **113**, 056602 (2014).

[25] M. M. Jadidi, J. C. Konig-Otto, S. Winnerl, A. B. Sushkov, H. D. Drew, T. E. Murphy, and M. Mittendorff, Nano Lett. **16**, 2734 (2016).

[26] N. W. Ashcroft and N. D. Mermin, *Solid State Physics* (Brooks/Cole, 1976).

[27] S. Das Sarma and Q. Li, Phys. Rev. B **87**, 235418 (2013).

[28] P. Di Pietro, M. Ortolani, O. Limaj, A. Di Gaspare, V. Giliberti, F. Giorgianni, M. Brahlek, N. Bansal, N. Koirala, S. Oh et al., Nat. Nanotechnol. **8**, 556 (2013).

[29] N. Koirala, M. Brahlek, M. Salehi, L. Wu, J. Dai, J. Waugh, T. Nummy, M. G. Han, J. Moon, Y. Zhu et al., Nano Lett. **15**, 8245 (2015).

[30] L. Wu, M. Salehi, N. Koirala, J. Moon, S. Oh, and N. P. Armitage, Science **354**, 1124 (2016).

[31] M. Brahlek, N. Koirala, M. Salehi, N. Bansal, and S. Oh, Phys. Rev. Lett. **113**, 026801 (2014).

[32] See Supplemental Material at [URL will be inserted by publisher] for the additional experiment and calculation details.

[33] J. Hebling, G. Almási, I. Z. Kozma, and J. Kuhl, Opt. Express **10**, 1161 (2002).

[34] C. P. Hauri, C. Ruchert, C. Vicario, and F. Ardana, Appl. Phys. Lett. **99**, 161116 (2011).

[35] G. Gallot and D. Grischkowsky, J. Opt. Soc. Am. B **16**, 1204 (1999).

[36] Q. Wu, M. Litz, and X. C. Zhang, Appl. Phys. Lett. **68**, 2924 (1996).

[37] V. Giannini, Y. Francescato, H. Amrania, C. C. Phillips, and S. A. Maier, Nano Lett. **11**, 2835 (2011).

[38] A. Ferlauto, G. Ferreira, J. M. Pearce, C. Wronski, R. Collins, X. Deng, and G. Ganguly, J. Appl. Phys. **92**, 2424 (2002).

[39] B. Cheng, T. Ohtsuki, D. Chaudhuri, S. Nakatsuji, M. Lippmaa, and N. Armitage, Nat. Commun. **8**, 2097 (2017).

[40] V. Lucarini, J. J. Saarinen, K.-E. Peiponen, and E. M. Vartiainen, *Kramers-Kronig relations in optical materials research* (Springer Science and Business Media, 2005).

[41] R. D. Averitt, G. Rodriguez, J. L. W. Siders, and S. A. Trugman, J. Opt. Soc. Am. B **17**,

327 (2000).

[42] J. C. Konig-Otto, M. Mittendorff, T. Winzer, F. Kadi, E. Malic, A. Knorr, C. Berger, W. A. de Heer, A. Pashkin, H. Schneider et al., Phys. Rev. Lett. **117**, 087401 (2016).

[43] D. Zhao, H. Hu, R. Haselsberger, R. A. Marcus, M.-E. Michel-Beyerle, Y. M. Lam, J.-X. Zhu, C. La-o-vorakiat, M. C. Beard, and E. E. M. Chia, ACS Nano **13**, 8826 (2019).

[44] B. Wunsch, T. Stauber, F. Sols, and F. Guinea, New J. Phys. **8**, 318 (2006).

[45] L. J. Sherry, S.-H. Chang, G. C. Schatz, R. P. V. Duyne, and B. J. W. Y. Xia, Nano Lett. **5**, 2034 (2005).

[46] J. Kim, H. Son, D. J. Cho, B. Geng, W. Regan, S. Shi, K. Kim, A. Zettl, Y. R. Shen, and F. Wang, Nano Lett. **12**, 5598 (2012).

[47] T. Low and P. Avouris, ACS Nano **8**, 1086 (2014).

[48] Z. Fei, G. O. Andreev, W. Bao, L. M. Zhang, S. M. A, C. Wang, M. K. Stewart, Z. Zhao, G. Dominguez, M. Thiemens et al., Nano Lett. **11**, 4701 (2011).

[49] H. Yan, Z. Li, X. Li, W. Zhu, P. Avouris, and F. Xia, Nano Lett. **12**, 3766 (2012).

[50] S. Link and M. A. El-Sayed, J. Phys. Chem. B **103**, 8410 (1999).

[51] M. J. Kale and P. Christopher, Science **349**, 587 (2015).

[52] J. Yan, Y. Zhang, P. Kim, and A. Pinczuk, Phys. Rev. Lett. **98**, 166802 (2007).

[53] H. Yan, T. Low, W. Zhu, Y. Wu, M. Freitag, X. Li, F. Guinea, P. Avouris, and F. Xia, Nat. Photonics **7**, 394 (2013).

[54] G. X. Ni, L. Wang, M. D. Goldflam, M. Wagner, Z. Fei, A. S. McLeod, M. K. Liu, F. Keilmann, B. Özyilmaz, A. H. Castro Neto et al., Nat. Photonics **10**, 244 (2016).

[55] M. Brahlek, N. Koirala, N. Bansal, and S. Oh, Solid State Commun. **215-216**, 54 (2015).

[56] M. Dressel and G. Grüner, *Electrodynamics of Solids* (Cambridge University Press,

2003).

[57] J. Horng, C.-F. Chen, B. Geng, C. Girit, Y. Zhang, Z. Hao, H. A. Bechtel, M. Martin, A. Zettl, M. F. Crommie et al., Phys. Rev. B **83**, 165113 (2011).

[58] R. Bistritzer and A. H. MacDonald, Phys. Rev. Lett. **102**, 206410 (2009).

[59] S. Winnerl, M. Orlita, P. Plochocka, P. Kossacki, M. Potemski, T. Winzer, E. Malic, A. Knorr, M. Sprinkle, C. Berger et al., Phys. Rev. Lett. **107**, 237401 (2011).

[60] M. T. Mihnev, F. Kadi, C. J. Divin, T. Winzer, S. Lee, C. H. Liu, Z. Zhong, C. Berger, W. A. de Heer, E. Malic et al., Nat. Commun. **7**, 11617 (2016).

[61] I. Kwak, M.-C. Lee, B. C. Park, C. H. Kim, B. Lee, C. W. Seo, J. Yamaura, Z. Hiroi, T. W. Noh, and K. W. Kim, Phys. Rev. B **100**, 144309 (2019).

[62] L. Cheng, C. La-o-vorakiat, C. S. Tang, S. K. Nair, B. Xia, L. Wang, J.-X. Zhu, and E. E. M. Chia, Appl. Phys. Lett. **104**, 211906 (2014).